Constructing BiOBr/g-C_3N_4/$Bi_2O_2CO_3$ Z-Scheme Photocatalyst With Enhanced Photocatalytic Activity

Biao Zhang
UESTC: University of Electronic Science and Technology of China
Yu Liu (poly1634@hotmail.com)
UESTC: University of Electronic Science and Technology of China https://orcid.org/0000-0001-6367-9637
Kanghong Zhou
UESTC: University of Electronic Science and Technology of China
Hongyu Zhu
UESTC: University of Electronic Science and Technology of China
Dongxu Gu
UESTC: University of Electronic Science and Technology of China
Wei Ge
UESTC: University of Electronic Science and Technology of China
Ying Gan
UESTC: University of Electronic Science and Technology of China
Jianyuan Hao
UESTC: University of Electronic Science and Technology of China

Research Article

Keywords: Semiconductor, BiOBr/g-C3N4/Bi2O2CO3, Z-scheme mechanism, photocatalysts

Posted Date: March 18th, 2021

DOI: https://doi.org/10.21203/rs.3.rs-309897/v1

Version of Record: A version of this preprint was published at Journal of Materials Science: Materials in Electronics on July 16th, 2021. See the published version at https://doi.org/10.1007/s10854-021-06565-3.

Abstract

Novel camellia-structured Z-scheme BiOBr/g-C_3N_4/$Bi_2O_2CO_3$ was simply prepared by a hydrothermal method and photodegraded Rhodamine B under visible light within 60 min with much higher degradation efficiency (98%) contrasted with pure BiOBr, g-C_3N_4 and $Bi_2O_2CO_3$. Radical trapping experiments exhibited the main reactive species ($\cdot O_2^-$) during degradation process. The formation of Z-scheme heterojunction improved rate of charge separation, enhanced absorption of visible light and thus promoted the photocatalytic activity. The Z-scheme heterojunction is a promising material for the removal of dye in effluents.

1 Introduction

Rhodamine B (Rh B), is a widely used bright red cationic dye, can be seriously harmful to environment and wildlife, and is mutagenic and cancer-causing to humans[1]. Developing high efficiency photocatalysis based on semiconductor has become a green technology to effectively degrade detrimental organic pollutants and solve environment issues[2, 3]. Graphitic carbon nitride (g-C_3N_4) with a metal-free, visible-light response and narrow band gap of 2.7 eV has been attractive as a photocatalyst[4, 5]. In addition, the conduction band (CB) potential of g-C_3N_4 is comparatively negative (-1.15 eV)[5], which can bring higher reduction capability to photoexcited electrons. However, high recombination of photon-generated carriers of pure g-C_3N_4 restricted the further application. A promising method is that constructing effective semiconductor Z-scheme heterojunctions to intensify photocatalytic activity by improving the efficiency of charge separation[6, 7]. For instance, Zhang group[8] has reported remarkable Z-scheme heterojunction Ag_3PO_4/g-C_3N_4/$MoSe_2$, exhibiting high photocatalytic activity and visible light absorption.

Hitherto, due to the appropriate band gap, unique electronic properties and the response to visible light, bismuth-based photocatalysts have also been attracted extensive attention[9]. All kinds of Bi-based photocatalysts have been investigated, such as BiO_2CO_3[10], $BiVO_4$[11], Bi_2WO_6[12], and BiOX (X = Cl, Br, I)[9]. Among them, BiO_2CO_3 as a member of Aurivillius-based oxide family, has a twisted layered structure, which can provide a smooth transfer path for photogenerated electrons and holes, exhibits excellent catalytic activity, good stability and low toxicity, and is a class of photocatalysts with application potential[10, 13]. Moreover, BiO_2CO_3 possesses a strongly positive valence band (VB) value at 3.63 eV[14] for oxidation of organic contaminants. Nevertheless, BiO_2CO_3 has a wide band gap, low utilization of visible light and low carrier separation efficiency[10], resulting in lower photocatalytic activity. Moreover, the BiOBr compound photocatalyst is easy to accumulate because of its lamellar structure, and can provide enough polarization space, suitable forbidden band width, high specific surface area and porosity, and thus has good photocatalytic activity[9, 15]. Furthermore, the layered structures and different solubility constants of BiO_2CO_3 and BiOBr are easier to bind by simple ion exchange[16], thereby improving separation of photogenerated carriers and photocatalytic activity.

In this work, considering the band position, advantages and disadvantages of BiOBr, g-C_3N_4, and $Bi_2O_2CO_3$, simple hydrothermal method was carried on to synthesis Z-scheme BiOBr/g-C_3N_4/$Bi_2O_2CO_3$ ternary heterojunction composite. The photocatalytic ability of Rh B degradation under visible light illumination was examined and the mechanism of the Z-scheme structure was eventually discussed.

2 Experimental

2.1 Synthesis of photocatalysts

The melamine was thermally polymerized at 550°C for 4 h at a heating rate of 2.5°C/min to prepare g-C_3N_4[17].

BiOBr/g-C_3N_4/$Bi_2O_2CO_3$ was prepared by simple hydrothermal method. Briefly, 0.485 g of $Bi(NO_3)_3{\cdot}5H_2O$, 0.119 g of KBr and 0.06 g of urea were dissolved in 40 ml deionized water and stirred for 1 h (suspension A). g-C_3N_4 (0.025 g, 0.05 g and 0.1 g) was dissolved in 30 ml deionized water and sonicated for 30 min (suspension B). The mixture of A and B was stirred for another 30 min. Then transfer to autoclave and react at 160°C for 24 h. The precipitates were washed with distilled water for three times and dried at 80°C for 12 h. The as-synthesized BiOBr/g-C_3N_4/$Bi_2O_2CO_3$ with 0.025g, 0.05g and 0.1g of g-C_3N_4 were named as 0.025CN, 0.05CN and 0.1CN, respectively. BiOBr (BOB) and $Bi_2O_2CO_3$ (BOC) were synthesized by hydrothermal method. The detail and other experimental sections are shown in supplementary information.

3 Results And Discussion

3.1 Structural analysis

XRD patterns in Fig. 1a displayed graphitic-like layered stacking g-C_3N_4 (JCPDS No. 87-1526), tetragonal BiOBr (JCPDS NO. 78–0348) and tetragonal phase $Bi_2O_2CO_3$ (JCPDS No. 41-1488)[18–20]. Characteristic peaks of BOB and BOC were observed in ternary composite while no peak of g-C_3N_4 was found due to the low contents and poor crystallinity of g-C_3N_4 in the composites. FTIR spectra were displayed in Fig. 1b. As for g-C_3N_4, stretching vibrations of N-H was observed at 3000–3400 cm^{-1}[21] and stretching vibration of C-N heterocycles was significantly showed at 1200–1600 cm^{-1}[22]. Furthermore, the characteristic peak at 808 cm^{-1} is attributed to the typical breathing mode of the triazine units[23]. The ternary heterojunction is no significant difference with the peak of g-C_3N_4, indicating that the structural integrity of carbon nitride in the ternary composites is stable.

3.2 Morphology and composition analysis

Figure 2 was the SEM images of the prepared photocatalysts. Pure g-C_3N_4 material showed typically irregular topography (Fig. 2a), BOB material exhibited layered rectangular plates (Fig. 2b) and BOC

material represented irregular lamellar (Fig. 2c). However, BiOBr/g-C_3N_4/$Bi_2O_2CO_3$ composite in Fig. 2d appeared totally different morphology with camellia-like shape, which was formed gradually with the content decrease of g-C_3N_4 (Fig. S1). The possible reason is that the BOB BOC and g-C_3N_4 can dispersed well and assembled to camellia-shape with more interface contact and specific surface in the presence of small amount of g-C_3N_4, which may contribute to the enhancement of the effective electrons and holes separation. The successful preparation of the ternary heterojunction can be demonstrated by the EDS spectrum of 0.025 CN composite, which shows the coexistence of C, O, N, Br and Bi (Fig. 2e).

3.3 Element state analysis

X-ray photoelectron spectroscopy (XPS) was used to confirm the valence state and elemental compositions of the 0.025CN catalyst. The characteristic signal of Br, Bi, C, N, and O can be easily observed from the full spectrum (Fig. 3a), which confirms the presence of these elements in this material. The two peaks at the binding energy of 69.0 eV and 69.9 eV can be belonged to Br $3d_{5/2}$ and Br $3d_{3/2}$ (Fig. 3b), indicating that Br^{-1} in the 0.025CN composite[24]. The peaks at 160.0 eV and 165.3 eV matched well with photoemission from Bi $4f_{7/2}$ and Bi $4f_{5/2}$ (Fig. 3c), which confirm the valence state of Bi^{3+} in the composite[19]. The spectrum of C 1s in Fig. 3d displayed three different peaks. These peak at 284.8 eV, 288.7 eV and 289.6 were corresponded to the adventitious carbon, N-C = N and O = C-O, respectively[25]. In Fig. 3e, the N 1s peak appeared at 398.9 eV, 400.1eV and 404.3 eV, which attributed to the tertiary nitrogen bonded to carbon atoms (N-$(C)_3$), the nitrogen atoms in triazine rings (C-N = C) and = NH groups, respectively[21]. The high-resolution spectra of oxygen implies the exist of lattice oxygen of Bi–O and C–O at binding energy value at 530.4 eV and 531.5 eV, respectively (Fig. 3f)[26].

3.4 Photocatalytic performance and active species

The photocatalytic properties of the as-prepared catalysts were evaluated by the degradation experiment of Rh B under visible light irradiation. As shown in Fig. 4a, the concentration of Rh B solution decreased gradually in the presence of catalysts as reaction time was increased. The catalyst of 0.025CN displayed enhanced photocatalytic activity and degraded 98% of Rh B dye in 60 min, which exhibited remarkable photocatalytic activity compared to other ternary catalysts (Table S1). The dynamics plots in Fig. 4b reveals the corresponding rate constant (k). The rate constants k of BOC, g-C_3N_4, BOB, 0.1CN, 0.05CN and 0.025CN were calculated to be 0.00115 min^{-1}, 0.00915 min^{-1}, 0.01548 min^{-1}, 0.02248 min^{-1}, 0.02669 min^{-1}, 0.06224 min^{-1}, respectively. The rate constant of the 0.025CN composite is about 51.1, 6.8 and 4.0 time than that of BOC g-C_3N_4, and BOB, it displayed the best photocatalytic property in the removal of Rh B.

In order to elucidate the photocatalytic mechanism, the trapping experiment of active species was performed. Isopropyl alcohol (IPA), benzoquinone (BQ), triethanolamine (EDTA-2Na) were used as trapping agents for ·OH, $\cdot O_2^-$, h^+ scavenger respectively. The photodegradation of Rh B was effectively inhibited by BQ in Fig. 4c, indicating that $\cdot O_2^-$ were the main active species.

3.5 Optical property and photocatalytic mechanism

Photoluminescence (PL) spectra is one of the valid methods to evaluated photocatalytic mechanism. In general, the lower PL peak intensity is caused by an increase in the efficiency of the photo-induced electron-hole separation[27]. In Fig. 4d, the obvious lower PL intensity of 0.025CN indicated the high catalytic activity. The optical absorption of the semiconductor materials was evaluated by UV-Vis DRS. Wider absorption spectrum range of 0.025CN was observed in Fig. 4e. In Fig. 4f, the band gap of pure g-C_3N_4, BiOBr and $Bi_2O_2CO_3$ were 2.31, 2.67 and 3.38 eV, respectively. Furthermore, the valence band (VB) and conduction band (CB) potentials can be calculated using the following equations[14]: $E_{VB} = \chi + 0.5E_g - E^c$, $E_{CB} = E_{VB} - E_g$. E^c represents energy of free electrons on the hydrogen scale (4.5eV). χ is absolute electronegativity of the semiconductor, being 4.67, 6.176 eV and 6.54 eV for g-C_3N_4, BiOBr, and $Bi_2O_2CO_3$ respectively[14, 18, 28]. The calculated E_{VB} of g-C_3N_4, BiOBr, and $Bi_2O_2CO_3$ are 1.33 eV, 3.02eV and 3.73 eV, respectively, and for E_{CB} are − 0.98 eV, 0.34 eV and 0.35 eV, respectively.

Based on the characteristic and experimental data discussed above, the photocatalytic mechanism of BiOBr/g-C_3N_4/$Bi_2O_2CO_3$ was proposed, and described in Fig. 5. BiOBr/g-C_3N_4/$Bi_2O_2CO_3$ could be stimulated by visible-light irradiation and photoinduced electrons (e^-) on the CB of BiOBr and $Bi_2O_2CO_3$ would migrate to the VB of g-C_3N_4, and then the e^- quickly recombine with the photo-generated holes (h^+) on the VB of g-C_3N_4 inside the Z-scheme heterojunction so that the photogenerated electrons and holes of composite was efficiently separated[29, 30]. The e^- in the CB of g-C_3N_4 can react with O_2 to produce reactive $\cdot O_2^-$ radicals due to the more negative CB of g-C_3N_4 compared with the potential of $O_2/\cdot O_2^-$ (-0.33eV)[31]. Meanwhile, the h^+ in the VB of BiOBr and $Bi_2O_2CO_3$ can react with H_2O to produce reactive ·OH radicals due to the more positive VB of BiOBr and $Bi_2O_2CO_3$ compared to the potential of $H_2O/\cdot OH$(+ 2.72eV)[32]. In hence, the ternary heterojunction produces $\cdot O_2^-$ and ·OH by visible-light illumination that can effectively degrade Rh B.

4 Conclusion

Double Z-scheme BiOBr/g-C_3N_4/$Bi_2O_2CO_3$ heterojunction photocatalysts was designed and successfully synthesized. The remarkable higher photocatalytic activity on Rh B degradation under visible-light was observed. By contrast with pristine BiOBr, g-C_3N_4 and $Bi_2O_2CO_3$, composites displayed high photocatalytic activity due to promoting efficient charge separation through the Z-scheme heterostructure design. This work provides a potential strategy in the treatment of environmental pollution and remediation.

Declarations

Acknowledgements

This work was supported by National Natural Sciences Fund of China (No. 31670979, No. 51273034) and Science and Technology Program of Sichuan Province (2019YFS0132).

References

1. T. Wang, S. Liu, W. Mao, Y. Bai, K. Chiang, K. Shah, J. Paz-Ferreiro, J. Hazard. Mater. **389**, 121827 (2020)
2. Z. Zhu, X. Tang, C. Ma, M. Song, N. Gao, Y. Wang, P. Huo, Z. Lu, Y. Yan, Appl. Surf. Sci. **387**, 366 (2016)
3. W. Wang, L. Wang, W. Li, C. Feng, R. Qiu, L. Xu, X. Cheng, G. Shao, Mater. Lett. **234**, 183 (2019)
4. M. Jourshabani, B.-K. Lee, Z. Shariatinia, Appl. Catal. B. 276, (2020)
5. B. Lin, H. An, X. Yan, T. Zhang, J. Wei, G. Yang, Appl. Catal. B **210**, 173 (2017)
6. C. Li, P. Zhang, R. Lv, J. Lu, T. Wang, S. Wang, H. Wang, J. Gong, Small **9**, 3951 (2013)
7. Q. Li, X. Zhao, J. Yang, C.J. Jia, Z. Jin, W. Fan, Nanoscale **7**, 18971 (2015)
8. H. Zhang, G. Tang, X. Wan, J. Xu, H. Tang, Appl. Surf. Sci. 530, (2020)
9. K. Sharma, V. Dutta, S. Sharma, P. Raizada, A. Hosseini-Bandegharaei, P. Thakur, P. Singh, J. Ind. Eng. Chem. **78**, 1 (2019)
10. Z. Ni, Y. Sun, Y. Zhang, F. Dong, Appl. Surf. Sci. **365**, 314 (2016)
11. Q. Qin, Q. Cai, W. Hong, C. Jian, W. Liu, Chem. Eng. J. **402**, 126227 (2020)
12. M.T.L. Lai, C.W. Lai, K.M. Lee, S.W. Chook, T.C.K. Yang, S.H. Chong, J.C. Juan, J. Alloys Compd. **801**, 502 (2019)
13. R. Chen, G. Cheng, M.H. So, J. Wu, Z. Lu, C.-M. Che, H. Sun, Mater. Res. Bull. **45**, 654 (2010)
14. Z. Liu, W. Gu, F. Teng, X. Yang, W. Jiang, J. Fluorine Chem. **236**, 109557 (2020)
15. X. Ren, X. Zhang, R. Guo, S. Zhang, L. Wang, X. Pu, Nanotechnology **31**, 495405 (2020)
16. F. Qiu, W. Li, F. Wang, H. Li, X. Liu, C. Ren, Colloids Surf. A **517**, 25 (2017)
17. Z. Pan, G. Zhang, X. Wang, Angew. Chem. Int. Ed. Engl. **58**, 7102 (2019)
18. K. Zhou, Y. Liu, J. Hao, Mater. Lett. **281**, 128463 (2020)
19. D. Majhi, K. Das, A. Mishra, R. Dhiman, B.G. Mishra, Appl. Catal. B **260**, 118222 (2020)
20. H. Huang, X. Li, J. Wang, F. Dong, P.K. Chu, T. Zhang, Y. Zhang, ACS Cata. **5**, 4094 (2015)
21. X. Jiang, S. Lai, W. Xu, J. Fang, X. Chen, J. Beiyuan, X. Zhou, K. Lin, J. Liu, G. Guan, J. Alloys Compd. **809**, 151804 (2019)
22. S.C. Yan, Z.S. Li, Z.G. Zou, Langmuir **25**, 10397 (2009)
23. M.J. Bojdys, J.O. Muller, M. Antonietti, A. Thomas, Chemistry **14**, 8177 (2008)
24. B. He, Y. Du, Y. Feng, M. Du, J. Wang, J. Qu, Y. Liu, N. Jiang, J. Wang, X. Sun, Appl. Surf. Sci. **506**, 145031 (2020)
25. Y. Lan, Z. Li, W. Xie, D. Li, G. Yan, S. Guo, C. Pan, J. Wu, J. Hazard. Mater. **385**, 121622 (2020)
26. J. Wang, X. Zhai, G. Zhang, J. Zhang, Y. Zhao, Solid State Sci. **105**, 106288 (2020)
27. M. Wang, P. Guo, T. Chai, Y. Xie, J. Han, M. You, Y. Wang, T. Zhu, J. Alloys Compd. **691**, 8 (2017)
28. X. Ren, K. Wu, Z. Qin, X. Zhao, H. Yang, J. Alloys and Compd. **788**, 102 (2019)

29. X. Miao, X. Yue, Z. Ji, X. Shen, H. Zhou, M. Liu, K. Xu, J. Zhu, G. Zhu, L. Kong, S.A. Shah, Appl. Catal. B **227**, 459 (2018)
30. Y. Shang, X. Chen, W. Liu, P. Tan, H. Chen, L. Wu, C. Ma, X. Xiong, J. Pan, Appl. Catal. B **204**, 78 (2017)
31. X. Zhang, J. Yan, L.Y.S. Lee, Appl. Catal. B **283**, 119624 (2021)
32. L. Jiang, X. Yuan, G. Zeng, J. Liang, X. Chen, H. Yu, H. Wang, Z. Wu, J. Zhang, T. Xiong, Appl. Catal. B **227**, 376 (2018)

Figures

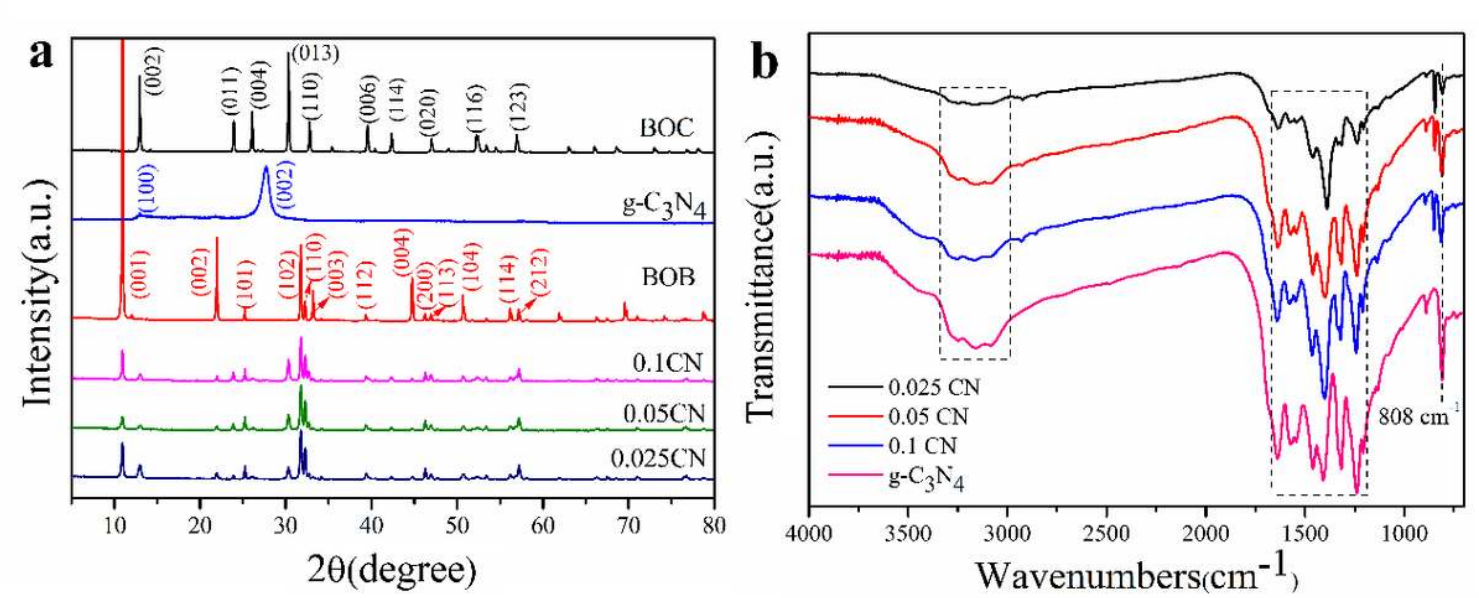

Figure 1

(a) XRD patterns of different samples, (b) FTIR spectra of 0.025CN, 0.05CN, 0.1CN and g-C3N4.

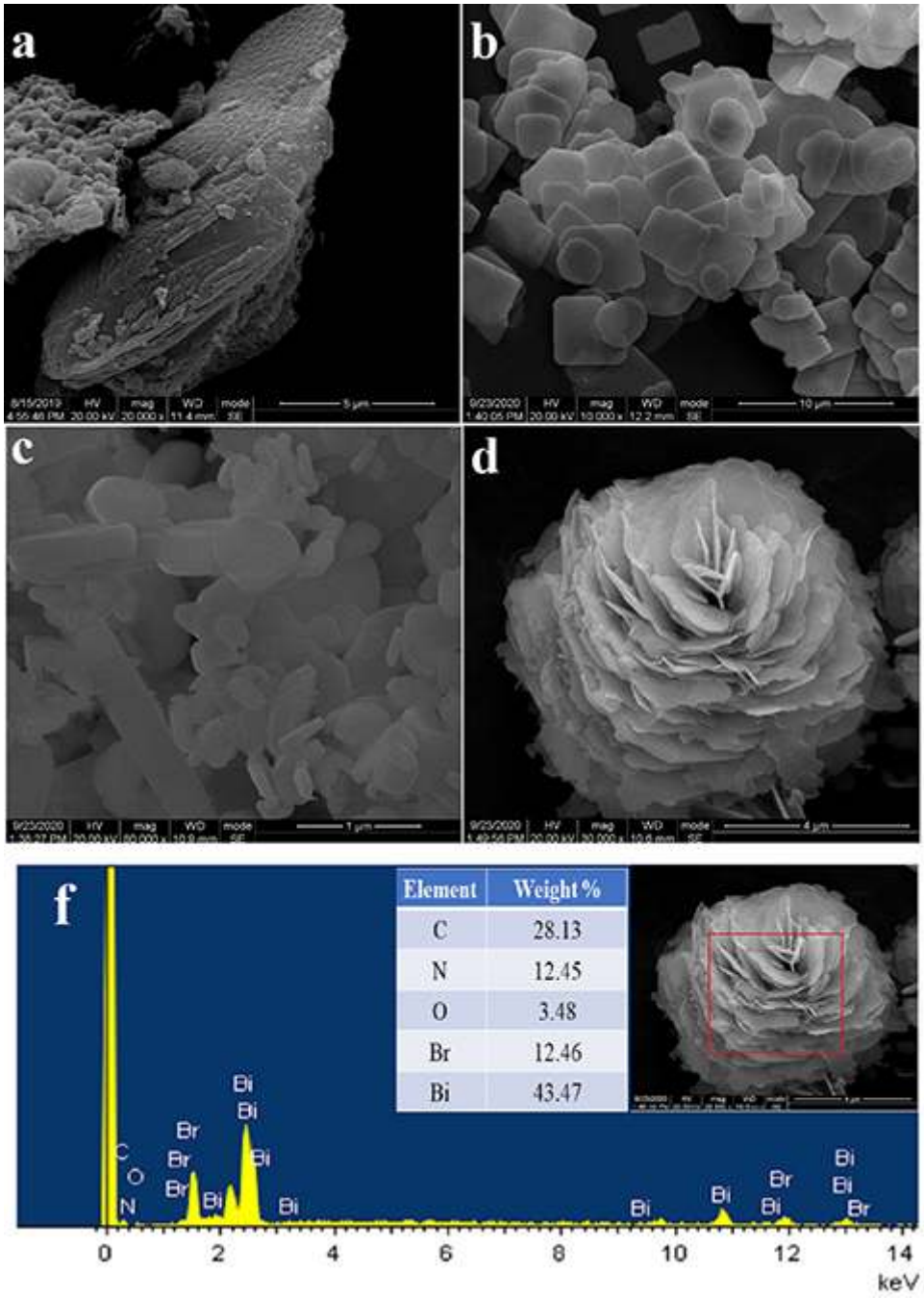

Figure 2

SEM images of (a) g-C3N4, (b) BOB, (c) BOC, (d) 0.025CN, (f) EDS of 0.025CN

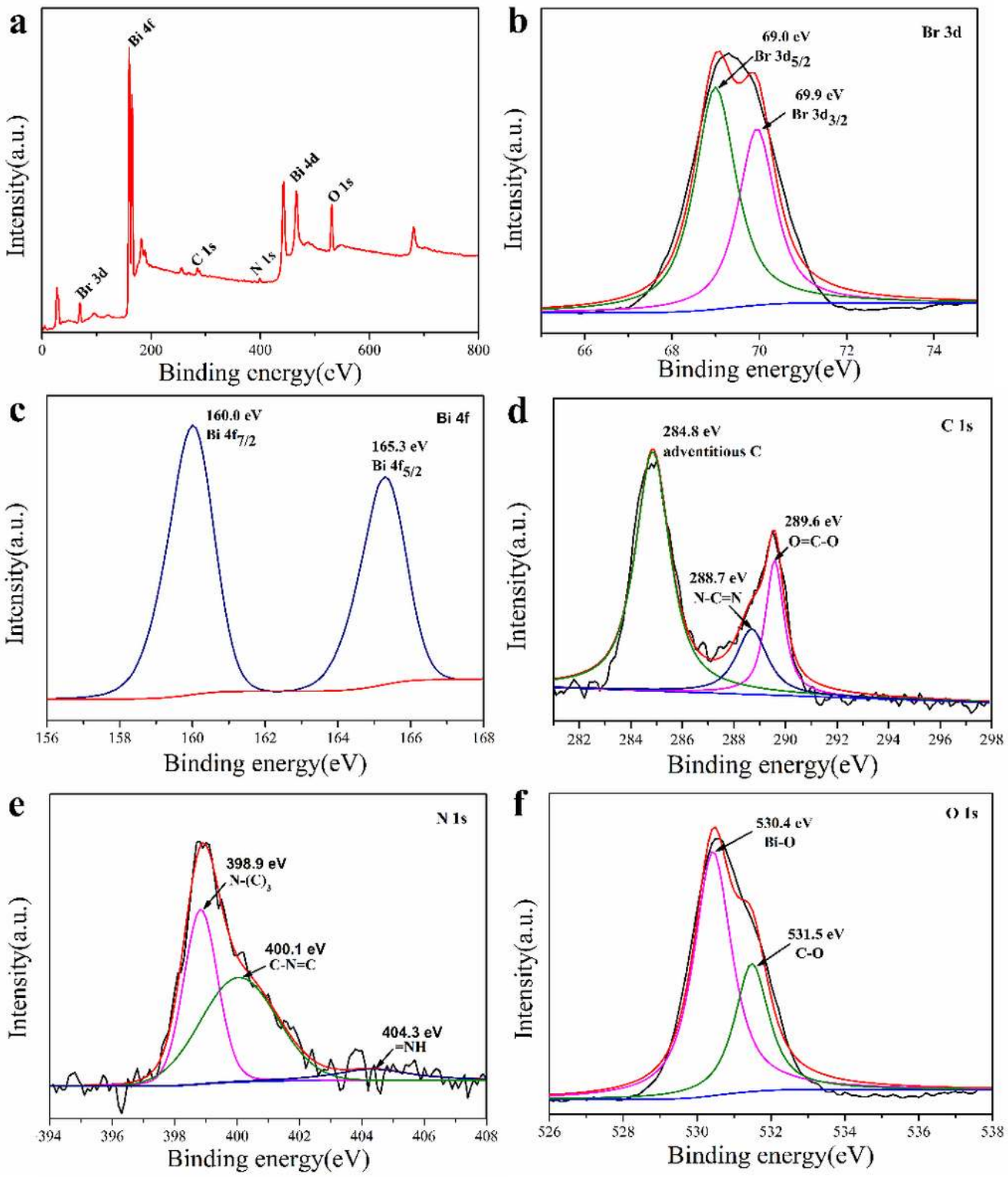

Figure 3

XPS spectra of 0.025CN: (a) full spectra, (b) Br 3d, (c) Bi 4f, (d) C 1s, (e) N 1s, and (f) O 1s.

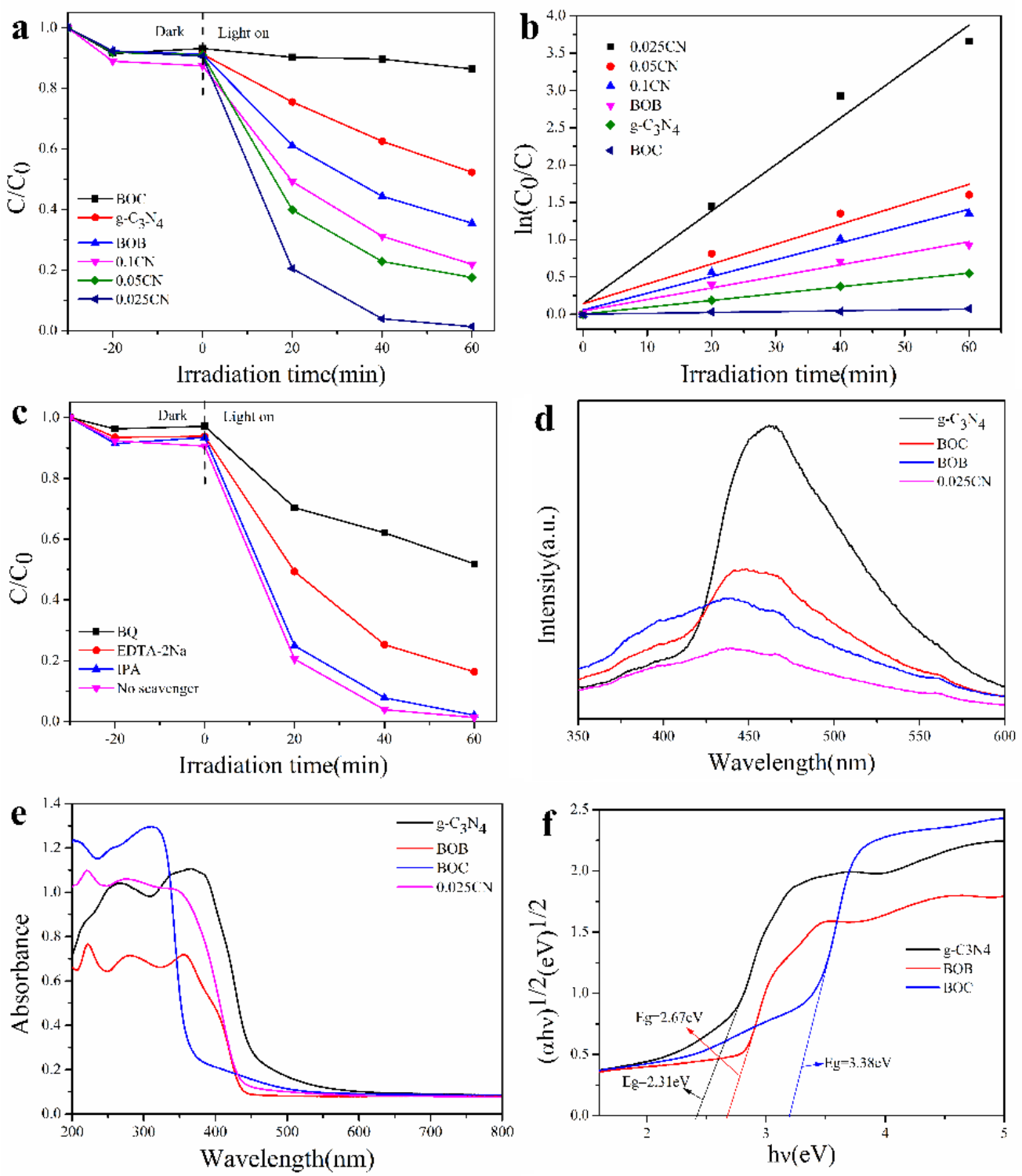

Figure 4

(a) Rh B degradation curves of samples, (b) Plots of ln(C0/C) versus time, (c) The species trapping experiments, (d) PL spectra, (e)UV–vis DRS spectra, (f) Band gap energies of g-C3N4, BOB and BOC.

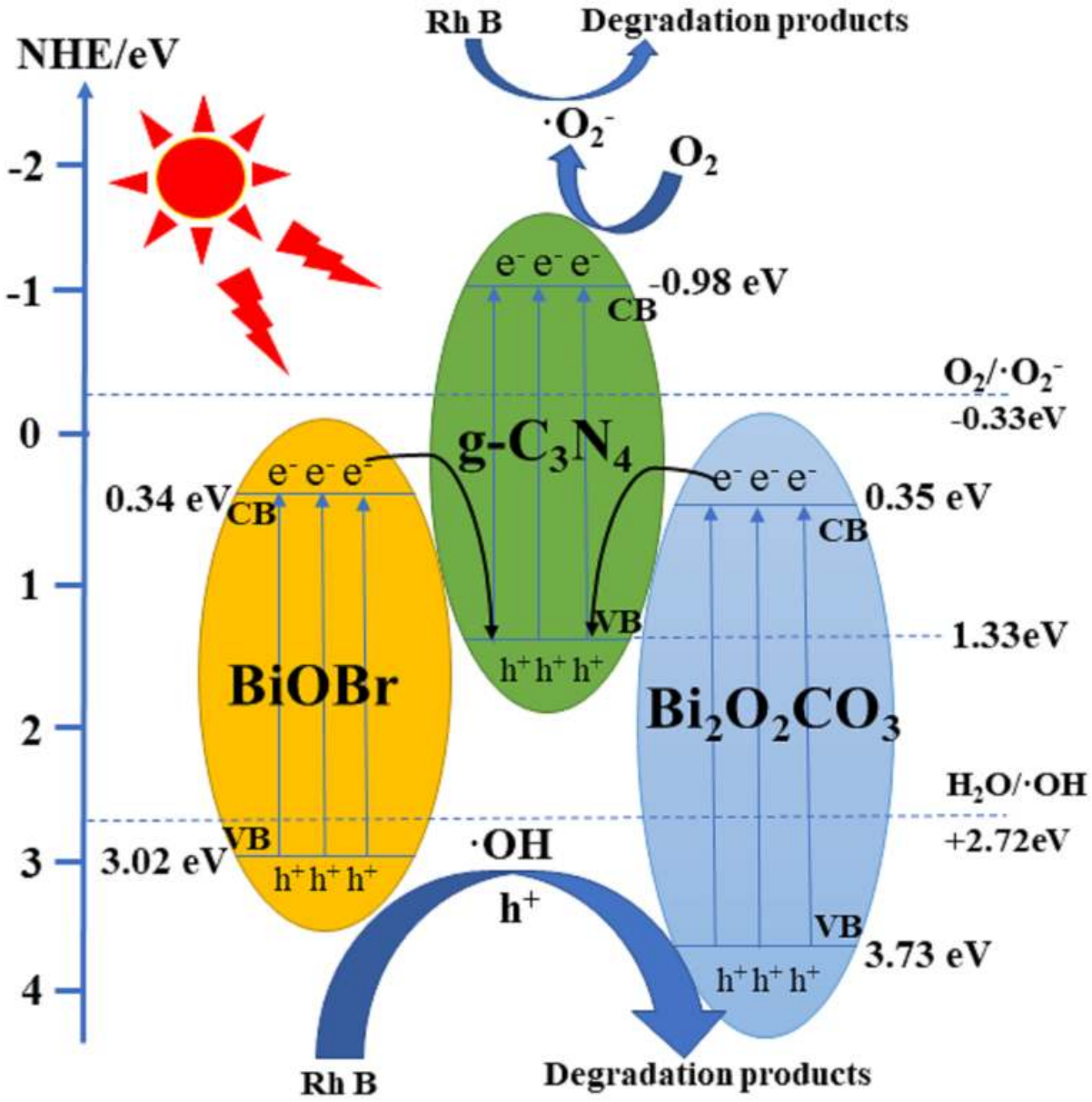

Figure 5

Proposed mechanism of BiOBr/g-C3N4/Bi2O2CO3 Z-scheme photocatalyst.

Supplementary Files

This is a list of supplementary files associated with this preprint. Click to download.

- SupplementaryInformation.docx